

## Hydroclimatic shifts in northeast Thailand during the last two millennia - the record of Lake Pa Kho

Chawchai, S., Chabangborn, A., Fritz, S., Väiliranta, M., Mörth, C-M., Blaauw, M., ... Wohlfarth, B. (2015). Hydroclimatic shifts in northeast Thailand during the last two millennia - the record of Lake Pa Kho. *Quaternary Science Reviews*, 111, 62-71. DOI: 10.1016/j.quascirev.2015.01.007

**Published in:**  
Quaternary Science Reviews

**Document Version:**  
Peer reviewed version

**Queen's University Belfast - Research Portal:**  
[Link to publication record in Queen's University Belfast Research Portal](#)

### **Publisher rights**

© 2015 Elsevier Ltd. All rights reserved.

This is an open access article published under a Creative Commons Attribution-NonCommercial-NoDerivs License (<https://creativecommons.org/licenses/by-nc-nd/4.0/>), which permits distribution and reproduction for non-commercial purposes, provided the author and source are cited.

### **General rights**

Copyright for the publications made accessible via the Queen's University Belfast Research Portal is retained by the author(s) and / or other copyright owners and it is a condition of accessing these publications that users recognise and abide by the legal requirements associated with these rights.

### **Take down policy**

The Research Portal is Queen's institutional repository that provides access to Queen's research output. Every effort has been made to ensure that content in the Research Portal does not infringe any person's rights, or applicable UK laws. If you discover content in the Research Portal that you believe breaches copyright or violates any law, please contact [openaccess@qub.ac.uk](mailto:openaccess@qub.ac.uk).

1 **Hydroclimatic shifts in northeast Thailand during the last two millennia – the record of**  
2 **Lake Pa Kho**

3 Sakonvan Chawchai<sup>\*1</sup>, Akkaneewut Chabangborn<sup>1,2</sup>, Sherilyn Fritz<sup>3</sup>, Minna Väiliranta<sup>4</sup>, Carl-  
4 Magnus Mörth<sup>1</sup>, Maarten Blaauw<sup>5</sup>, Paula J. Reimer<sup>5</sup>, Paul J. Krusic<sup>6</sup>, Ludvig Löwemark<sup>7</sup> &  
5 Barbara Wohlfarth<sup>\*1</sup>

6 <sup>1</sup>*Department of Geological Sciences, Stockholm University, Stockholm 10691, Sweden*

7 <sup>2</sup>*Department of Geology, the Faculty of Science, Chulalongkorn University, Bangkok 10330,*  
8 *Thailand*

9 <sup>3</sup>*Department of Earth and Atmospheric Sciences and School of Biological Sciences,*  
10 *University of Nebraska-Lincoln 68588-0340, USA*

11 <sup>4</sup>*Department of Environmental Sciences, University of Helsinki, Helsinki 4603, Finland*

12 <sup>5</sup>*Centre for Climate, the Environment & Chronology (14CHRONO), School of Geography,*  
13 *Archaeology and Palaeoecology, Queen's University of Belfast, Belfast BT7 1NN, UK*

14 <sup>6</sup>*Department of Physical Geography and Quaternary Geology, Stockholm University,*  
15 *Stockholm 10691, Sweden*

16 <sup>7</sup>*Department of Geosciences, National Taiwan University, Taipei 106, Taiwan*

17

18

19 <sup>\*</sup>Corresponding Authors: Sakonvan Chawchai and Barbara Wohlfarth

20 Department of Geological Sciences, Stockholm University, Stockholm 10691, Sweden

21 E-mail: [sakonvan.chawchai@geo.su.se](mailto:sakonvan.chawchai@geo.su.se); [barbara.wohlfarth@geo.su.se](mailto:barbara.wohlfarth@geo.su.se)

22

23

24

25

26

27 **ABSTRACT**

28 The Southeast Asian mainland is located in the central path of the Asian summer monsoon, a  
29 region where paleoclimatic data are still sparse. Here we present a multi-proxy (TOC, C/N,  
30  $\delta^{13}\text{C}$ , biogenic silica, and XRF elemental data) study of a 1.5 m sediment/peat sequence from  
31 Lake Pa Kho, northeast Thailand, which is supported by 20 AMS  $^{14}\text{C}$  ages. Hydroclimatic  
32 reconstructions for Pa Kho suggest a strengthened summer monsoon between BC 170 - AD  
33 370, AD 800-960, and after AD 1450; and a weakening of the summer monsoon between AD  
34 370-800, and AD 1300-1450. Increased run-off and a higher nutrient supply after AD 1700  
35 can be linked to agricultural intensification and land-use changes in the region. This study fills  
36 an important gap in data coverage with respect to summer monsoon variability over Southeast  
37 Asia during the past 2000 years and enables the mean position of the Intertropical  
38 Convergence Zone (ITCZ) to be inferred based on comparisons with other regional studies.  
39 Intervals of strengthened/weaker summer monsoon rainfall suggest that the mean position of  
40 the ITCZ was located as far north as  $35^\circ\text{N}$  between BC 170-AD 370 and AD 800-960,  
41 whereas it likely did not reach above  $17^\circ\text{N}$  during the drought intervals of AD 370-800 and  
42 AD 1300-1450. The spatial pattern of rainfall variation seems to have changed after AD 1450,  
43 when the inferred moisture history for Pa Kho indicates a more southerly location of the mean  
44 position of the summer ITCZ.

45 **Key words:**

46 Wetland/peatland; geochemistry; paleoclimate; last two millennia; Asian Monsoon

47 **Highlights**

48 New high-resolution  $^{14}\text{C}$ -dated, multi-proxy peat sequence from NE Thailand

49 Reconstruction of hydroclimatic variability during the past 2000 years

50 Strengthened Asian summer monsoon BC 170-AD 370 and AD 800-970

51 Weaker Asian summer monsoon AD 370-800 and AD 1300-1450

52 Shifts in the mean position of the summer ITCZ during the past 2000 years

53 **1. Introduction**

54 The Asian summer monsoon during the past 2000 years was generally weaker than in the  
55 early Holocene in response to the long-term decline in summer insolation (Y. Wang et al.,  
56 2005). Yet high-resolution tree ring (Cook et al., 2010), marine (Anderson et al., 2002;  
57 Newton et al., 2006; Oppo et al., 2009), coral (Cobb et al., 2003), speleothem (Sinha et al.,  
58 2011a; Zhang et al., 2008), and lake (Yancheva et al., 2007) studies show that substantial  
59 decadal to centennial variations in summer monsoon intensity were superimposed on the  
60 long-term trend. Various hypotheses have been brought forward to explain this decadal to  
61 centennial scale variability, including solar forcing (Zhang et al., 2008); El Niño Southern  
62 Oscillation (ENSO) (Cobb et al., 2003; Mann et al., 2009) and Indo-Pacific climate variability  
63 (Prasad et al., 2014; Ummenhofer et al., 2013); movement of the mean position of the  
64 Intertropical Convergence Zone (ITCZ) (Newton et al., 2006; Sachs et al., 2009; Tierney et  
65 al., 2010); and changes in the Indian Ocean Dipole (Ding et al., 2010; Ummenhofer et al.,  
66 2013) and Pacific Walker Circulation (Yan et al., 2011).

67

68 The most detailed reconstructions of decadal and sub-decadal shifts in summer monsoon  
69 strength are derived from the network of Asian tree ring sites (MADA) extending back  
70 through the last millennium (Cook et al., 2010; Pages 2K Consortium, 2013). MADA and key  
71 speleothem records from China and India suggest, for example, a general weakening of the  
72 summer monsoon between AD 1400–1800 and a link between intense droughts during the  
73 14<sup>th</sup> and 15<sup>th</sup> centuries and the demise of ancient societies in various parts of Asia (Buckley et  
74 al., 2010, 2014; Sinha et al., 2011b; Zhang et al., 2008).

75 The Asian monsoon system is comprised of several sub-systems whose modern interactions  
76 are complex, with considerable spatial variation in monsoon intensity and frequency (P. Wang  
77 et al., 2005; Wang, 2009). The Indian, the East Asian, and the Western North Pacific summer

78 monsoon subsystems influence the Southeast Asian mainland, but how these systems  
79 interacted to affect the spatial pattern of past drought is not well resolved. Tree ring records  
80 generally span less than 1000 years and have gaps in spatial coverage, and other  
81 palaeoenvironmental data for the Southeast Asian mainland are still sparse. Thus, additional  
82 regional records are critical to fully resolve spatial patterns of Asian monsoon variation during  
83 the late Holocene, a key step in understanding long-term monsoon dynamics and potential  
84 monsoon responses to changing global climate conditions.

85 Here we develop a high-resolution palaeoenvironmental data series (TOC, C/N,  $\delta^{13}\text{C}$ ,  
86 biogenic silica, and XRF elemental data) supported by 20 accelerator mass spectrometer  
87 (AMS)  $^{14}\text{C}$  ages, from a 1.5 m long sediment/peat sequence from Lake Pa Kho in northeast  
88 Thailand (Fig. 1A). The site is located close to the present boundary between the East Asian  
89 and Indian Ocean monsoon domains at  $105^\circ\text{E}$  (P. Wang et al., 2005), and is affected by the  
90 seasonal migration of the summer monsoon and of the ITCZ.

91

## 92 **2.1 Regional setting**

93 Lake Pa Kho ( $17^\circ 06' \text{N}$ ,  $102^\circ 56' \text{E}$ ; 175 m above sea level;  $<3 \text{ km}^2$ ) is presently a dammed  
94 lake that flooded a former wetland (Penny, 2001). Several dams (built between 1989 and  
95 2004) divide the lake into three sub-basins of different size (Fig. 1B). Low hills to the west  
96 and south rise to  $\sim 230$  m above sea level (Fig. 1B) and are the source of small seasonal  
97 streams that feed neighboring Lake Kumphawapi. The flat area surrounding the lake is  
98 primarily used as paddy fields, and for sugar cane and *Eucalyptus* plantations. The bedrock  
99 underlying the alluvial sediments is mainly composed of Cretaceous and Neogene sand and  
100 siltstones (El Tabakh et al., 2003; Wannakomol, 2005).

101 Climate in the region is tropical monsoonal, with mean air temperatures of  $\sim 22^{\circ}$  to  $25^{\circ}\text{C}$  from  
102 November to February and  $27^{\circ}$  to  $30^{\circ}\text{C}$  from March to October (Fig. 1C). Mean annual  
103 precipitation is  $\sim 1455$  mm, 88% of which falls from May to October. Thailand's  
104 tropical/subtropical monsoon shows a strong correlation with indices of the Indian summer  
105 monsoon and the Western North Pacific summer monsoon during the instrumental period  
106 (Limsakul et al., 2011). From 1980 to 2011, subdecadal and decadal weakening of the  
107 summer monsoon in Thailand has also been associated with ENSO variability, specifically  
108 with the increasing number of El Niño events (Bridhikitti, 2013; Hsu et al., 2014; Singhrattna  
109 et al., 2005).

110 Prior reconstructions of the regional paleoenvironment based on pollen and spore studies from  
111 a 2.30 m long sequence of Lake Pa Kho (Penny 1998, 2001) showed vegetation changes at the  
112 Pleistocene/Holocene transition (ca. 12000-10000 cal yr BP), with the expansion of tropical  
113 and sub-tropical broad-leaf taxa in response to the development of relatively humid climatic  
114 conditions (Penny, 2001, 1998). However, this reconstruction (Penny 1998, 2001) did not  
115 extend into the late Holocene and did not provide information on hydroclimatic conditions and  
116 vegetation change after 5000 cal yr BP. The absence of late-Holocene sediments suggests  
117 that the earlier coring location either did not accumulate or did not preserve the most recent  
118 history of the site.

### 119 **3. Materials and methods**

120 During fieldwork in January 2010, two overlapping 10-m long sequences were cored in the  
121 central part of the southern basin (Fig. 1B) using a modified Russian corer (7.5 cm diameter, 1  
122 m length). The core sections were described in the laboratory, and each 1-m-long core  
123 segment was scanned with the Itrax XRF core scanner at 5 mm resolution using a Mo tube set  
124 at 30 kV and 30 mA for 60 sec/point. Distinct lithological markers and ITRAX scanning

125 results were used to correlate between parallel core segments, thus creating a composite  
126 stratigraphy for coring point CP3. The sequence of 2.00-3.50 meter depth below the water  
127 surface is the focus of this study and was subdivided into five lithostratigraphic units (Table  
128 1). Consecutive samples comprising 1-cm intervals were freeze-dried. The part between 3.50  
129 and 11.00 m depth is still being analyzed (Chabangborn, 2014).

130 Selected elemental data (Si, K, and Ti) obtained from XRF scanning were averaged over 1 cm  
131 intervals and then normalized by (incoherent + coherent) scattering to remove various  
132 instrumental effects (Kylander et al., 2011). Si, K and Ti are here used as proxies for mineral  
133 input.

134 For further geochemical analyses, each freeze-dried and ground sample (150 samples in total)  
135 was weighed into a tin capsule for analysis with an elemental analyzer (Carlo Erba NC2500)  
136 connected to a Finnigan MAT Delta+ mass spectrometer. Total organic carbon (TOC) and  
137 total nitrogen (TN) were measured in weight percentage, and their values are interpreted as  
138 productivity indicators. C/N ratios are expressed as atomic ratios. In lake sediments these  
139 ratios allow discrimination between aquatic and terrestrial organic matter sources (Meyer and  
140 Teranes, 2001; Meyers, 2003). In peatlands, however, C/N ratios may indicate changes in the  
141 type of peat-forming plants (Kuhry and Vitt, 1996) and/or are an indicator of the degree of  
142 peat decomposition (Chimner and Ewel, 2005).  $\delta^{13}\text{C}_{\text{org}}$  values are reported in parts per  
143 thousand (permil, ‰) relative to the Vienna PeeDee Belemnite (VPDB, for C), with an  
144 analytical error of  $\pm 0.15\%$ , and are here used as a proxy for the contribution of aquatic versus  
145 terrestrial plants (Meyer and Teranes, 2001; Meyers, 2003).

146 To assess the productivity of siliceous microfossils, 51 samples were selected for analysis of  
147 biogenic silica (BSi) and pre-cleaned with  $\text{H}_2\text{O}_2$  and HCl to remove organic matter and  
148 carbonate. The BSi content was determined by alkaline extraction of 30 mg of material in 40

149 mL of 1% Na<sub>2</sub>CO<sub>3</sub> solution over a 5 hour period, with sub-samples taken at 3 (within), 4 and  
150 5 hours and neutralized with 0.21N HCl. The extracts were analyzed for dissolved silica (DSi)  
151 by ICP-OES (Varian Vista Ax), and the concentration data were plotted against depth/time.  
152 The easily soluble phases (e.g. diatom frustules, phytoliths) are dissolved within two hours.  
153 Crystalline phases (silicate minerals) take a longer time to dissolve. Through calculating a  
154 linear regression between the 3, 4 and 5 hour measurements of DSi values, we can  
155 differentiate the biogenic silica dissolved. The value where the linear regression crosses the  
156 vertical axis (the y-intercept) of the sub-sample plots was considered to be the BSi (wt %)  
157 corrected for a simultaneous dissolution of silica from minerals. Based on peaks in the BSi  
158 curve, 15 sub-samples were further analyzed to estimate the relative contribution of diatoms  
159 and phytoliths. Much of the sample material had however already been used for other  
160 analyses; therefore the diatom/phytolith analyses are not continuous. Sub-samples for diatom  
161 and phytolith analysis were treated with 10% HCl to remove any carbonates and heated in  
162 H<sub>2</sub>O<sub>2</sub> to oxidize organic matter. An aliquot of each sample was dried onto a cover slip, which  
163 was mounted onto a glass slide using a permanent mounting medium (Zrax or Naphrax).

164 The chronostratigraphy is based on 20 AMS <sup>14</sup>C ages (Table 2; Fig. 2B, C). Sieve remains  
165 (mesh size 0.5 mm) of the samples were identified under a stereomicroscope and rinsed  
166 multiple times in deionized water. Samples with a sufficient amount of plant remains  
167 (charcoal, seeds, leaves, insects, and small wood fragments) were chosen for dating. The  
168 selected samples were dried overnight at 105°C in pre-cleaned glass vials and sent to the  
169 <sup>14</sup>CHRONO Centre at Queen's University, Belfast for analysis. The sieve residues of 9  
170 samples were further examined for macroscopic plant remains and charcoal. The plant  
171 assemblage types were described, and the depositional environment was classified as  
172 aquatic/open water, telmatic (larger plant fragments originating from e.g. reeds, sedges and  
173 horsetails), or terrestrial (Table 1, Fig. 3).



174 The radiocarbon age and one standard deviation were calculated using the Libby half-life of  
175 5568 years and a fractionation correction based on  $\delta^{13}\text{C}$  measured on the AMS (Table 2). The  
176 age-model was constructed using Bacon, a Bayesian statistics-based routine that models  
177 accumulation rates by dividing a sequence into many thin segments and estimating the (linear)  
178 accumulation rate for each segment based on the (calibrated)  $^{14}\text{C}$  dates, together with  
179 assumptions about accumulation rate and its variability between neighboring segments  
180 (Blaauw and Christen, 2011). Prior to selecting the present age models (CP3\_82,  
181 CP3\_82\_hiatus) (Fig. 2B, C), multiple model runs were performed using different  
182 assumptions and parameters.

183

## 184 **4. Results**

### 185 4.1. Chronology

186 The  $^{14}\text{C}$  dates for CP3 plot sequentially according to depth, but two  $^{14}\text{C}$  dates (UBA-19841 at  
187 3.40-3.44 m and UBA-23312 at 2.78-2.83 m) have older ages than expected (Table 2, Fig. 2B,  
188 C) and are treated as outliers by Bacon. Sequential samples UBA-14636 (2.66-2.63 m) and  
189 UBA-19839 (2.63-2.60 m) differ in age by c. 460 calibrated  $^{14}\text{C}$  years (Table 2). Explanations  
190 for this age difference between adjoining levels include low accumulation rates or the  
191 presence of a hiatus. The stratigraphy, TOC, C/N ratio, elemental data and plant macrofossil  
192 composition give no indication for an abrupt change or a hiatus at 2.63 m depth, but  $\delta^{13}\text{C}$  and  
193 BSi values show a distinct shift (Table 1, Fig. 3).

194 We therefore constructed two age models; one assuming low accumulation rates (CP3\_82)  
195 around 2.63 m, and one assuming the presence of a hiatus (CP3\_82\_hiatus) (Fig. 2B, C). Both  
196 age models provide similar ages for the sequence below 2.68 m depth and above 2.63 m

197 depth, but result in a different duration (510 and 170 years, respectively) for the depth interval  
198 between 2.68 and 2.63 m. Lower accumulation rates between 2.68 and 2.63 m (AD 840-1320)  
199 as shown in the age model of CP3-82 (Fig. 2B) are inconsistent with the deposition of fibrous  
200 and less decomposed peat. The  $\delta^{13}\text{C}_{\text{org}}$  values of -22 to 23‰ and occurrence of aquatic-  
201 telmatic plants also suggest the availability of water and conditions favorable for peat  
202 accumulation (Fig. 3). Age model CP3\_82\_hiatus on the other hand implies continuous  
203 accumulation between 2.68 and 2.63 m depth (AD 800-970), followed by a 330 year long  
204 hiatus (Fig. 2 C). Since peat accumulation below and above 2.63 m depth occurred at a similar  
205 rate in both age models, a sudden slowdown in accumulation rate between 2.68 and 2.63 m, at  
206 the same time as  $\delta^{13}\text{C}_{\text{org}}$  increase and plant remains suggest wetland conditions, seems  
207 difficult to reconcile. Our preferred hypothesis is therefore to include a hiatus at 2.63 m depth.

#### 208 4.2. Stratigraphy and geochemistry of Pa Kho

209 The stratigraphy of CP3 shows from bottom to top a fine detritus gyttja, peaty gyttja, peat and  
210 loose organic sediments (Table 1). The overall high TOC content of the sequence suggests  
211 high organic production (Fig. 3).

212  $\delta^{13}\text{C}_{\text{org}}$  values (-24 to -21‰) in the lowermost fine detritus and peaty gyttja (3.50-3.04 m  
213 depth; BC 170 - AD 370) indicate that the sediments contain a mix of aquatic, telmatic and  
214 terrestrial organic material (Fig. 3). Macroscopic plant remains and the presence of diatoms  
215 and phytoliths would support this. C/N ratios of 27-24, however, point to a predominantly  
216 terrestrial organic carbon source (Meyer and Teranes, 2001; Meyers, 2003) and suggest,  
217 together with elevated values for Si, K, and Ti, that run-off was important. Taken together, the  
218 proxy data indicate that Pa Kho was a shallow productive lake or a wetland with areas of open  
219 water between BC 170 and AD 370.

220 The transition from peaty gyttja to compact peat at AD 370 coincides with a distinct decrease  
221 in  $\delta^{13}\text{C}_{\text{org}}$  values from -23 to -28‰, an increase in BSi (phytoliths) and the occurrence of  
222 terrestrial plant remains (Fig. 3).  $\delta^{13}\text{C}_{\text{org}}$  values remain low between 3.04 and 2.98 m (AD  
223 370-410), increase again to -24‰ between 2.98 and 2.93 m (AD 410-450), and display low,  
224 but fluctuating values of -30 to -27‰ until 2.68 m (AD 800). The overall gradual decrease in  
225 the C/N ratio, which starts at 2.93 m (AD 450), may be explained by peat decomposition. This  
226 process liberates soluble carbon compounds, whereas nitrogen remains relatively constant,  
227 because most of its labile forms have already been consumed or transformed to inorganic  
228 forms (Chimner and Ewel, 2005; Ise et al., 2008). Charcoal was observed between 2.98 and  
229 2.73 m (AD 410-650), and the sample analyzed for plant remains between 2.78-2.73 m (AD  
230 580-650) is composed of terrestrial-telmatic species (Fig. 3). The different proxies thus  
231 suggest the development of a peatland between AD 370 and 800, but also that conditions may  
232 have been variable, with a lower water table and lower effective moisture between AD 370-  
233 410 and between AD 450-800, and slightly higher moisture availability between AD 410-450.

234 The marked increase in  $\delta^{13}\text{C}_{\text{org}}$  values to -21‰ at 2.68 m and the shift from terrestrial-telmatic  
235 to telmatic-aquatic plant assemblages at 2.66 m (Fig. 3) point to the re-establishment of a  
236 wetland at Pa Kho, and thus to higher effective moisture between AD 800 and 970. The  
237 subsequent hiatus suggested by the age model (CP\_82\_hiatus) at 2.63 m depth implies that  
238 330 years are 'missing' in our record. Such a gap in a peat sequence can be caused by  
239 decomposition and oxidation of the organic material under aerobic conditions. Although the  
240 different processes affecting tropical peatlands are still poorly understood, a recent laboratory  
241 experiment shows that drought can lead to considerable carbon loss in tropical peat samples  
242 (Fenner and Freeman, 2011). Indeed, the lowest  $\delta^{13}\text{C}_{\text{org}}$  values (-28‰) and the peak in BSi  
243 (phytoliths) just above the hiatus, i.e. between 2.63-2.62 m (AD 1300-1340) (Fig. 3), suggest  
244 an expansion of terrestrial plants onto the former wetland and generally lower effective

245 moisture, which persisted until 2.58 m (AD 1450). In contrast, the telmatic-aquatic plant  
246 assemblage between 2.63 and 2.60 m points to a water-saturated peat surface. This  
247 discrepancy can, however, be explained by the fact that each geochemical sample covers a  
248 one-centimeter interval, while the macrofossil sample corresponds to a three-centimeter  
249 interval and thus incorporates a mixed signal (Fig. 3). A lower and/or fluctuating water table  
250 would have led to exposure of the peat surface, and consequently to oxidation and/or  
251 biodegradation of the underlying organic material that had been accumulating between AD  
252 970 and 1300.

253 The gradual increase in  $\delta^{13}\text{C}_{\text{org}}$  values to -22‰ after AD 1450 (Fig. 3) and the macroscopic  
254 plant remains show that telmatic-aquatic plant material contributed to the organic carbon pool.  
255  $\delta^{13}\text{C}_{\text{org}}$  values remain constant (-24 and -25‰) between 2.51-2.02 m (AD 1510-2001), and the  
256 presence of the diatom species *Eunotia yanomami*, *Eunotia incisa*, *Eunotia intermedia*,  
257 *Eunotia monodon*, and *Gomphonema gracile* coupled with the plant macrofossil composition  
258 indicate a wetland environment.

259 The stepwise increase in BSi content at 2.31 m (AD 1700) and 2.07 m depth (AD 1960) may  
260 signify higher nutrient availability, and the distinct increase in major elements (Si, K, Ti) at  
261 2.17 m depth (AD 1850) and at 2.05 m depth (AD 1970) is likely related to land-use changes  
262 around Pa Kho (Klubseang, 2011). This would suggest a significant human impact, which  
263 overprints any climate signal. The historical record around the region is not well documented,  
264 but the change seen in the Pa Kho's sequence after AD 1700 coincides with the start of  
265 agricultural intensification in SE Asia (Lieberman and Buckley, 2012). The high C/N ratio  
266 (22), high  $\delta^{13}\text{C}$  values (-22‰) and peaks of BSi, diatom and elemental data (Si, K, Ti) during  
267 the last 10 years are likely the result of the dam and intensified cultivation around the lake.

268

## 269 **5. Discussion**

270 The sedimentary proxies show that Pa Kho was a shallow productive lake or wetland between  
271 BC 170 and AD 370. Such an environment implies high effective moisture, likely caused by a  
272 strengthened summer monsoon. Around AD 370 the wetland transformed to a peatland with a  
273 lower water table, which suggests a decrease in effective moisture and a weakening of the  
274 summer monsoon. This transition occurred in a stepwise fashion, given that alternating  
275 intervals of lower effective moisture (AD 370-410), slightly higher effective moisture (AD  
276 420-450) and lower effective moisture (until AD 800) are inferred (Fig. 4c). The re-  
277 establishment of a wetland between AD 800 and 970 is a sign of higher effective moisture and  
278 likely reflects increased summer monsoon precipitation. The subsequent hiatus (AD 970-  
279 1300) might have been caused by degradation of the peat surface during an interval with  
280 lower effective moisture and a weakened summer monsoon (AD 1300-1450) (Fig. 4c). The  
281 increase in aquatic plant remains, the appearance of diatoms and the isotope proxies show  
282 again a wetland environment starting around AD 1450. This marks a return to higher effective  
283 moisture and a moderately strengthened summer monsoon. The geochemical proxies  
284 established for CP3 can be compared with the multi-sediment and multi-proxy records of  
285 Lake Kumphawapi, which is located 15 km to the northeast. These showed the re-  
286 establishment of a shallow lake around AD 150-350 and suggested higher effective moisture  
287 and a strengthened summer monsoon (Chawchai et al., 2013; Wohlfarth et al., 2012), similar  
288 to our interpretation of the Pa Kho record. However, a detailed interpretation of the  
289 paleoenvironment in Kumphawapi after AD 350 is limited due to chronological uncertainties.

290 Given the lack of paleo-precipitation records from tropical lakes and wetland in Southeast  
291 Asia, it is important to examine whether the environmental signals stored in Pa Kho's  
292 sequence are a reflection of summer monsoon variability. To infer spatial patterns of

293 hydroclimatic variability, we compare the Pa Kho data set to selected high-resolution  
294 paleoclimatic records established for the Asian monsoon region. The stronger/weaker summer  
295 monsoon intervals presented in Figures 4 a-f follow the interpretation of the respective  
296 authors and present a fairly coherent picture of Asian summer monsoon variability. The  
297 terrestrial plant leaf wax ( $\delta D_{\text{wax}}$ ) record established from marine sediments from the Makassar  
298 Strait, Southwest Sulawesi (Tierney et al., 2010) is the only high-resolution record extending  
299 as far back as Pa Kho, while the Wanxiang Cave  $\delta^{18}\text{O}$  data set commences around AD 200  
300 (Zhang et al. 2008). All other high-resolution records only cover the last 1400 years (central  
301 India composite record) (Berkelhammer et al. 2010; Sinha et al. 2011a, 2011b, 2007); the last  
302 1000 years (Dongdao Island) (Yan et al., 2011) or the past 700-800 years (MADA data set;  
303 Dayu Cave) (Buckley et al., 2007, 2010, 2014; Cook et al., 2010; Tan et al., 2009) (Fig. 4a-f).

304 Higher effective moisture (BC 170 – AD 370), followed by a stepwise decline (AD 370-450)  
305 and lower moisture availability (AD 450-800) as reconstructed for Pa Kho is comparable with  
306 the  $\delta^{18}\text{O}$  record from Wanxiang Cave in central China (Fig. 4a, c). This record suggests that  
307 the summer monsoon was moderately strong between AD 190-530, gradually declined after  
308 AD 530 and was markedly weaker between AD 860-940 (Zhang et al., 2008) (Fig. 4a, c). The  
309 offset of 60 to 140 years between the two data sets at the beginning and end of the weaker  
310 summer monsoon period, respectively, may stem from chronological uncertainties. Upwelling  
311 indicators (*Globigerina bulloides*) in sediments from the northwestern Arabian Sea also show  
312 a weakening of the summer monsoon starting around AD 450 (Anderson et al., 2010, 2002),  
313 and the composite speleothem  $\delta^{18}\text{O}$  records from Indian caves give evidence for decadal  
314 intervals of a distinctly weaker summer monsoon between AD 650-900 (Berkelhammer et al.,  
315 2010; Sinha et al., 2011a, 2007) (Fig. 4b). These time intervals of a stronger/weaker Asian  
316 summer monsoon, however, differ from to the  $\delta D_{\text{wax}}$  record from the Makassar Strait (Fig. 4a-

317 c, f), which suggests a weaker Asian monsoon until around AD 450 and subsequently a  
318 stronger monsoon until about AD 1000 (Tierney et al., 2010) (Fig. 4f).

319 Berkelhammer et al. (2010), Sinha et al. (2011a, 2007) and Zhang et al. (2008) infer a  
320 strengthening of the summer monsoon between AD 950-1300 from speleothem  $\delta^{18}\text{O}$  records  
321 (Fig. 4a, b). These findings are comparable within error margins to our data set, which  
322 suggests higher effective moisture starting around AD 800 (Fig. 4c), but they differ from  
323 lower precipitation inferred over Dongdao Island in the South China Sea between AD 1000-  
324 1400 (Yan et al., 2011) (Fig. 4d).  $\delta D_{\text{wax}}$  values from the Makassar Strait also imply a weaker  
325 summer monsoon throughout the period AD 1000-1350 (Tierney et al., 2010) (Fig. 4f).

326 The Pa Kho data set gives evidence for distinctly lower effective moisture between AD 1300  
327 and 1450. This coincides, within error margins, with the start of a weaker summer monsoon  
328 phase recorded in Wanxiang Cave (Zhang et al., 2008) (Fig. 4a), and also compares to the  
329 intervals of lower precipitation (AD 1249-1325; 1390-1420) inferred from speleothem  $\delta^{18}\text{O}$   
330 values in Dayu Cave (Tan et al., 2009). Decreased upwelling in the Arabian Sea (AD 1350-  
331 1550) is also interpreted as a weakening of the Asian summer monsoon (Anderson et al.,  
332 2010, 2002). Distinct decadal-long droughts are recognized in the  $\delta^{18}\text{O}$  records of Indian cave  
333 speleothems between AD 1300-1450 (Berkelhammer et al., 2010; Sinha et al., 2011a, 2011b,  
334 2007), in the MADA tree-ring data set (AD 1340-1370; 1400-1425) and in the sediment  
335 proxies from the West Baray reservoir at Angkor, Cambodia (AD 1300-1400) (Buckley et al.,  
336 2007, 2010; Cook et al., 2010; Day et al., 2012) (Fig. 4b, e). The Dongdao Island (Yan et al.,  
337 2011, 2011) and Makassar Strait (Tierney et al. 2010) records on the other hand imply a shift  
338 towards a strengthened summer monsoon around AD 1350-1400 (Fig. 4d, f).

339 The inferred moisture history for Pa Kho since AD 1450 (Fig. 4c) compares well to the  
340 moderately intense summer monsoon reconstructed from Indian cave speleothems

341 (Berkelhammer et al., 2010; Sinha et al., 2011a, 2011b, 2007) and Arabian Sea proxies  
342 (Anderson et al., 2010, 2002), but seems to diverge from the hydroclimatic scenario  
343 established for Wanxiang Cave (Zhang et al. 2008). A correspondence can also be found  
344 between the Pa Kho record and climate inferences for Dongdao Island and southwest  
345 Sulawesi, where higher precipitation has been reconstructed since AD 1400 (Fig. 4d, f)  
346 (Tierney et al., 2010; Yan et al., 2011). It is interesting, however, to note that the  
347 interpretation of the speleothem  $\delta^{18}\text{O}$  records from Wanxiang Cave (Zhang et al., 2008) and  
348 neighboring Dayu Cave (Tan et al., 2009) do not correspond to each other. For Wanxiang  
349 Cave, a generally weaker summer monsoon is reconstructed throughout the time interval AD  
350 1350-1850 (Zhang et al., 2008), whereas the Dayu Cave record suggests a weaker summer  
351 monsoon around AD 1300-1400, an increase in summer monsoon intensity around AD 1500,  
352 intervals of higher monsoon precipitation between AD 1535-1685, AD 1755-1835 and AD  
353 1920-1970, and lower precipitation between AD 1890-1915 (Tan et al., 2009). When Li et al.  
354 (2014) compared speleothem  $\delta^{18}\text{O}$  records from a region spanning from  $60^\circ$  to  $125^\circ\text{E}$  and  
355 from  $10^\circ$  to  $40^\circ\text{N}$ , they observed similar and divergent precipitation patterns in close-by  
356 speleothem records from China. This would suggest that monsoon precipitation on decadal  
357 and centennial time scales varied regionally and that the response to climate change between  
358 and within each monsoon sub-system is complicated. The obvious differences between the  
359 two speleothem data sets starting around AD 1500 would imply that speleothem  $\delta^{18}\text{O}$  values  
360 do not provide a straightforward measure for large-scale regional summer monsoon intensity,  
361 but that they also record sub-regional precipitation signals, or that a number of other factors  
362 are involved in creating the  $\delta^{18}\text{O}$  signal (Li et al., 2014).

363 Sinha et al. (2011) note a distinct shift in precipitation patterns around AD 1650-1700, when  
364  $\delta^{18}\text{O}$  values from caves in northern and central India start to diverge. Records from central  
365 India suggest a shift from drier to wetter conditions, while the northern Indian caves indicate a



366 shift from wetter to drier conditions. This shift in precipitation patterns has been interpreted as  
367 reflecting active and break phases of the Indian summer monsoon (Sinha et al., 2011a). The  
368 decadal droughts during the 17<sup>th</sup> and 18<sup>th</sup> centuries registered in Indian cave speleothems  
369 (Berkelhammer et al., 2010; Sinha et al., 2011a, 2011b, 2007) and in the MADA data set  
370 (Buckley et al., 2007, 2010, 2014; Cook et al., 2010; D'Arrigo et al., 2011; Sano et al., 2009)  
371 are not recognized in the Pa Kho proxies (Fig. 4 b-e). This is likely due to the lower temporal  
372 resolution as compared to the tree-ring and speleothem records, but it could also be that  
373 human impact overprinted any climatic signals.

374 The opposing hydroclimatic patterns seen between Wanxiang Cave and Pa Kho in the north  
375 and southwest Sulawesi in the south can be explained by their location relative to the  
376 migration of the ITCZ (Sinha et al., 2011b; Tierney et al., 2010), and by interactions between  
377 the Asian-Australian monsoon systems. A strengthened Asian summer monsoon between BC  
378 170 - AD 500 and between AD 900-1300, in combination with a weak Australian monsoon,  
379 would have led to a shift of the tropical rain belt northward of Indonesia, leading to drought in  
380 equatorial regions. The opposite would have been the case between AD 500-900 and between  
381 AD 1300-1450, when the Asian summer monsoon weakened and the mean position of the  
382 tropical rain belt shifted over Indonesia. This hydroclimatic scenario seems to have changed  
383 after AD 1450, when the two neighboring Chinese cave records show opposing dry/wet  
384 patterns, the northeast Indian cave speleothems a shift to dry conditions and the central Indian  
385 caves a shift to wetter condition, while Pa Kho shows patterns similar to those on Dongdao  
386 Island and in Southwest Sulawesi (Fig. 4a-f). Independent of the differences between  
387 Wanxiang and Dayu Caves, which could stem from local factors, we may assume that the  
388 effect of a moderately strengthened summer monsoon was only registered as far north as 20°  
389 N, while rainfall was strong over the equatorial region. We thus hypothesize that the mean  
390 summer position of the ITCZ over land did not reach as far north as during the strengthened

391 summer monsoon intervals before AD 1450 and that it was located approximately where it is  
392 today (Fig. 5). Similar conclusions have been drawn based on a record from the central  
393 equatorial Pacific (Sachs et al., 2009).

394 Decadal drought intervals during the past 700-800 years seen in the in the MADA tree ring  
395 data series and in Dayu Cave speleothems have been linked to ENSO variability (Cook et al.  
396 2010; Tan et al. 2009). However, the moisture history derived from Wanxiang Cave has been  
397 associated with solar influence and climate variability in the North Atlantic region (Zhang et  
398 al. 2008). Decadal drought observed in the Indian speleothems, on the other hand, have been  
399 linked to Indian Ocean variability (Sinha et al. 2011). The centennial-scale shifts in  
400 hydroclimatic conditions reconstructed for Pa Kho support shifts in the mean position of the  
401 ITCZ as these produced associated changes in summer monsoon precipitation. IOD and  
402 ENSO events also may have had important influences on monsoon rainfall on decadal time  
403 scales, but these are not clearly registered in our centennial- scale record.

404 A more precise reconstruction of the temporal and spatial variability of past monsoon  
405 precipitation patterns and their underlying causes would require several additional high-  
406 resolution hydroclimatic records from the Asian monsoon region. Only a dense network of  
407 well-dated, multi-proxy data sets can help to reduce the current uncertainties in interpretation  
408 and provide a valid base for evaluating the inherent leads and lags of different proxies used to  
409 infer hydroclimatic conditions.

410

## 411 **Conclusions**

412 The new hydroclimatic reconstruction based on the high-resolution data set established for  
413 Lake Pa Kho in northeast Thailand adds important information in data coverage between  
414 China and Indonesia during the last two millennia. The multi-proxy study of the Pa Kho

415 sequence reveals time intervals when the summer monsoon was strengthened (BC 170-AD  
416 370, AD 800 – 960, and since AD 1450) and time intervals of drought (AD 370–800 and AD  
417 1300-1450). Within error margins the effective moisture variability (BC 170 – AD 1450)  
418 reconstructed for Pa Kho is comparable to hydroclimatic patterns derived from speleothem  
419 proxies in China and India. The drought intervals expressed in these records compare to  
420 intervals of stronger monsoonal rainfall in equatorial regions, as shown by the record from the  
421 Makassar Strait in Indonesia. This hydroclimatic pattern seems to have changed sometime  
422 between AD 1450-1600, when the inferred moisture history for Pa Kho became more similar  
423 to that reconstructed for the South China Sea and the Indonesian region. This would suggest  
424 that the mean position of the ITCZ over land generally did not reach as far north as it did prior  
425 to AD 1450.

426

#### 427 **Acknowledgments**

428 We thank Rienk H. Smittenberg and Kweku Afrifa Yamoah for discussions about the  
429 geochemistry and Francesco Muschitiello for discussions about age models. Kevin J.  
430 Anchukaitis and Karina Schollaen provided the SE Asian tree ring data sets and Hong Yan  
431 those for Cattle Pond. Jan Risberg, and Shyhrete Shala helped with the diatom and phytolith  
432 analyses and Wichuratree Klubseang provided the digital file, which was used to draw the  
433 map in Figure 1B. Heike Sigmund and the Stable Isotope Laboratory at the Department of  
434 Geological Sciences, Stockholm University are acknowledged for analyzing total and CN  
435 isotopes. Research in Thailand was financed through Swedish Research Council (VR)  
436 research grants 621-2008-2855 and 348-2008-6071. S. Chawchai acknowledges financial  
437 support from the Royal Thai Government Scholarship under the DPST project.

438

439 **Figure text**

440 **Figure 1.** (A) Location of the study area in northeast Thailand. (B) Topography around Pa  
441 Kho and the location of coring point CP3. The coordinate system is based on the UTM Grid  
442 system (WGS 1984 zone 48; asl = above sea level). (C) Mean monthly rainfall and  
443 temperature (1962-2011) for Udon Thani, which is situated 36 km NW of Pa Kho. Map (A)  
444 was generated using the generic mapping tools-GMT (<http://gmt.soest.hawaii.edu/>), and map  
445 (B) was redrawn based on aerial photographs before and after 1994 using the data set in  
446 Klubseang (2011).

447 **Figure 2.** (A) Lithostratigraphy for CP3, (B) age model CP3\_82 and (C) age model  
448 CP3\_82\_hiatus. The blue shapes show the calibrated  $^{14}\text{C}$  dates with two standard deviations,  
449 the grey shading indicates the likely age model and the dotted lines show the 95% confidence  
450 ranges of the age model. See Table 1 for a detailed description of the sequence and Table 2  
451 for the  $^{14}\text{C}$  dates.

452 **Figure 3.** Lithostratigraphy, geochemistry, and selected elemental data for CP3. The samples  
453 analyzed for diatoms, phytoliths, charcoal, and plant macrofossil composition are  
454 discontinuous (see text for further explanations). Light gray bars represent higher effective  
455 moisture, and the dark gray bars represent lower effective moisture.

456 **Figure 4.** Selected high-resolution records for the Asian monsoon region for the past 2000  
457 years: (a)  $\delta^{18}\text{O}$  data of Wanxiang Cave speleothems (Zhang et al., 2008); (b) Composite  $\delta^{18}\text{O}$   
458 time series for central India based on speleothems from Dandak, Jhumar, and Wah Shikar  
459 Caves (Berkelhammer et al. 2010; Sinha et al. 2011a, 2011b, 2007); (c)  $\delta^{13}\text{C}_{\text{org}}$  data from  
460 Lake Pa Kho (this study); (d) grain size variations in sediment core DY6-MGS of Cattle  
461 Pond, Dongdao Island (Yan et.al, 2011); (e) Palmer Drought Severity Index (PDSI) derived  
462 from the Monsoon Asia Drought Atlas (MADA) for the region between 10-20°N and 95-

463 115°E (Buckley et al., 2007, 2010, 2014; Cook et al., 2010; D'Arrigo et al., 2011; Sano et al.,  
464 2009); (f)  $\delta D_{\text{wax}}$  from marine cores 31MC and 34GGC from southwest Sulawesi (Tierney et  
465 al., 2010). The vertical light gray bars represent higher effective moisture/a strengthened  
466 summer monsoon, and the dark gray bars represent lower effective moisture/a weakened  
467 summer monsoon. Note that the timing of the shifts in moisture history of the individual  
468 records follows that cited by the respective author/s. See Figure 5 for the location of the  
469 different records.

470 **Figure 5.** Location of selected high-resolution Asian monsoon paleo-records for the last 2000  
471 years. The mean position of the winter and summer Intertropical Convergence Zone (ITCZ) is  
472 according to Wang (2009). The July-August wind directions and wind speeds follow Wang et  
473 al. (2003). Long arrows indicate high wind speed and short arrows lower wind speed.

474

## 475 **Table text**

476 **Table 1.** Lithostratigraphic description, plant macrofossil composition of selected samples  
477 and inferred depositional environment for CP3.

478

479 **Table 2**  $^{14}\text{C}$  dates for CP3. Core depth (in m) is given below the water surface. See Figure 1  
480 for the location of the coring point. The stratigraphic units relate to those shown in Table 1.

481

## 482 **References**

- 483 Anderson, D.M., Baulcomb, C.K., Duvivier, A.K., Gupta, A.K., 2010. Indian summer  
484 monsoon during the last two millennia. *Journal of Quaternary Science* 25, 911–917.  
485 doi:10.1002/jqs.1369
- 486 Anderson, D.M., Overpeck, J.T., Gupta, A.K., 2002. Increase in the Asian Southwest  
487 Monsoon During the Past Four Centuries. *Science* 297, 596–599.  
488 doi:10.1126/science.1072881

- 489 Berkelhammer, M., Sinha, A., Mudelsee, M., Cheng, H., Edwards, R.L., Cannariato, K.,  
490 2010. Persistent multidecadal power of the Indian Summer Monsoon. *Earth and*  
491 *Planetary Science Letters* 290, 166–172. doi:10.1016/j.epsl.2009.12.017
- 492 Blaauw, M., Christen, J., 2011. Flexible paleoclimate age-depth models using an  
493 autoregressive gamma process. *Bayesian Analysis* 6, 457–474.
- 494 Bridhikitti, A., 2013. Connections of ENSO/IOD and aerosols with Thai rainfall anomalies  
495 and associated implications for local rainfall forecasts. *International Journal of*  
496 *Climatology* 33, 2836–2845. doi:10.1002/joc.3630
- 497 Buckley, B., Palakit, K., Duangsathaporn, K., Sanguantham, P., Prasomsin, P., 2007. Decadal  
498 scale droughts over northwestern Thailand over the past 448 years: links to the tropical  
499 Pacific and Indian Ocean sectors. *Climate Dynamics* 29, 63–71. doi:10.1007/s00382-  
500 007-0225-1
- 501 Buckley, B.M., Anchukaitis, K.J., Penny, D., Fletcher, R., Cook, E.R., Sano, M., Nam, L.C.,  
502 Wichienkeo, A., Minh, T.T., Hong, T.M., 2010. Climate as a contributing factor in  
503 the demise of Angkor, Cambodia. *Proceedings of the National Academy of Sciences*  
504 107, 6748–6752. doi:10.1073/pnas.0910827107
- 505 Buckley, B.M., Fletcher, R., Wang, S.-Y.S., Zottoli, B., Pottier, C., 2014. Monsoon extremes  
506 and society over the past millennium on mainland Southeast Asia. *Quaternary Science*  
507 *Reviews* 95, 1–19. doi:10.1016/j.quascirev.2014.04.022
- 508 Chabangborn, A., 2014. Asian monsoon over mainland Southeast Asia in the past 25000  
509 years. PhD Thesis, Stockholm University, Stockholm, Sweden, 65pp.
- 510 Chawchai, S., Chabangborn, A., Kylander, M., Löwemark, L., Mörth, C.-M., Blaauw, M.,  
511 Klubseang, W., Reimer, P.J., Fritz, S.C., Wohlfarth, B., 2013. Lake Kumphawapi – an  
512 archive of Holocene palaeoenvironmental and palaeoclimatic changes in northeast  
513 Thailand. *Quaternary Science Reviews* 68, 59–75.  
514 doi:10.1016/j.quascirev.2013.01.030
- 515 Chimner, R.A., Ewel, K.C., 2005. A Tropical Freshwater Wetland: II. Production,  
516 Decomposition, and Peat Formation. *Wetlands Ecology and Management* 13, 671–  
517 684. doi:10.1007/s11273-005-0965-9
- 518 Cobb, K.M., Charles, C.D., Cheng, H., Edwards, R.L., 2003. El Niño/Southern Oscillation  
519 and tropical Pacific climate during the last millennium. *Nature* 424, 271–276.  
520 doi:10.1038/nature01779
- 521 Cook, E.R., Anchukaitis, K.J., Buckley, B.M., D’Arrigo, R.D., Jacoby, G.C., Wright, W.E.,  
522 2010. Asian Monsoon Failure and Megadrought During the Last Millennium. *Science*  
523 328, 486–489. doi:10.1126/science.1185188
- 524 D’Arrigo, R., Palmer, J., Ummenhofer, C.C., Kyaw, N.N., Krusic, P., 2011. Three centuries  
525 of Myanmar monsoon climate variability inferred from teak tree rings. *Geophysical*  
526 *Research Letters* 38, L24705. doi:10.1029/2011GL049927
- 527 Day, M.B., Hodell, D.A., Brenner, M., Chapman, H.J., Curtis, J.H., Kenney, W.F., Kolata,  
528 A.L., Peterson, L.C., 2012. Paleoenvironmental History of the West Baray, Angkor  
529 (Cambodia). *Proceedings of the National Academy of Sciences* 109, 1046–1051.  
530 doi:10.1073/pnas.1111282109
- 531 El Tabakh, M., Utha-Aroon, C., Warren, J.K., Schreiber, B.C., 2003. Origin of dolomites in  
532 the Cretaceous Maha Sarakham evaporites of the Khorat Plateau, northeast Thailand.  
533 *Sedimentary Geology* 157, 235–252. doi:10.1016/S0037-0738(02)00235-X
- 534 Fenner, N., Freeman, C., 2011. Drought-induced carbon loss in peatlands. *Nature Geoscience*  
535 4, 895–900. doi:10.1038/geo1323
- 536 Hsu, H.-H., Zhou, T., Matsumoto, J., 2014. East Asian, Indochina and Western North Pacific  
537 Summer Monsoon - An update. *Asia-Pacific Journal of Atmospheric Sciences* 50, 45–  
538 68. doi:10.1007/s13143-014-0027-4

- 539 Ise, T., Dunn, A.L., Wofsy, S.C., Moorcroft, P.R., 2008. High sensitivity of peat  
540 decomposition to climate change through water-table feedback. *Nature Geoscience* 1,  
541 763–766. doi:10.1038/ngeo331
- 542 Klubseang, W., 2011. Paleogeography and paleoenvironment of Nong Han Kumphawapi,  
543 Changwat Udon Thani. MSc thesis Chulalongkorn University, Bangkok 1–110.
- 544 Kuhry, P., Vitt, D.H., 1996. Fossil Carbon/Nitrogen Ratios as a Measure of Peat  
545 Decomposition. *Ecology* 77, 271–275. doi:10.2307/2265676
- 546 Kylander, M.E., Ampel, L., Wohlfarth, B., Veres, D., 2011. High-resolution X-ray  
547 fluorescence core scanning analysis of Les Echets (France) sedimentary sequence:  
548 new insights from chemical proxies. *Journal of Quaternary Science* 26, 109–117.  
549 doi:10.1002/jqs.1438
- 550 Li, Y., Wang, N., Zhou, X., Zhang, C., Wang, Y., 2014. Synchronous or asynchronous  
551 Holocene Indian and East Asian summer monsoon evolution: A synthesis on Holocene  
552 Asian summer monsoon simulations, records and modern monsoon indices. *Global  
553 and Planetary Change* 116, 30–40. doi:10.1016/j.gloplacha.2014.02.005
- 554 Lieberman, V., Buckley, B., 2012. The Impact of Climate on Southeast Asia, circa 950–1820:  
555 New Findings. *Modern Asian Studies FirstView*, 1–48.
- 556 Limsakul, A., Paengkaew, W., Kummueang, A., Limjirakan, S., Suttamanuswong, B., 2011.  
557 PDSI-based variations of droughts and wet spells in Thailand: 1951–2005.  
558 *Environment Asia* 4, 12–20.
- 559 Mann, M.E., Zhang, Z., Rutherford, S., Bradley, R.S., Hughes, M.K., Shindell, D., Ammann,  
560 C., Faluvegi, G., Ni, F., 2009. Global Signatures and Dynamical Origins of the Little  
561 Ice Age and Medieval Climate Anomaly. *Science* 326, 1256–1260.  
562 doi:10.1126/science.1177303
- 563 Meyer, P.A., Teranes, J., 2001. Sediment organic matter. In: Last, W.M., Smol, J.P. (EDs),  
564 Tracking Environmental Change Using Lake Sediments: Physical and Geochemical  
565 Methods. Dordrecht.
- 566 Meyers, P.A., 2003. Applications of organic geochemistry to paleolimnological  
567 reconstructions: a summary of examples from the Laurentian Great Lakes. *Organic  
568 Geochemistry* 34, 261–289. doi:10.1016/S0146-6380(02)00168-7
- 569 Newton, A., Thunell, R., Stott, L., 2006. Climate and hydrographic variability in the Indo-  
570 Pacific Warm Pool during the last millennium. *Geophysical Research Letters* 33,  
571 L19710. doi:10.1029/2006GL027234
- 572 Oppo, D.W., Rosenthal, Y., Linsley, B.K., 2009. 2,000-year-long temperature and hydrology  
573 reconstructions from the Indo-Pacific warm pool. *Nature* 460, 1113–1116.  
574 doi:10.1038/nature08233
- 575 Pages 2K, Consortium, 2013. Continental-scale temperature variability during the past two  
576 millennia. *Nature Geoscience* 6, 339–346. doi:10.1038/ngeo1797
- 577 Penny, D., 1998. Late Quaternary Palaeoenvironments in the Sakon Nakhon Basin, North-east  
578 Thailand. PhD Thesis, Monash University, Victoria/Australia, 260pp.
- 579 Penny, D., 2001. A 40,000 year palynological record from north-east Thailand; implications  
580 for biogeography and palaeo-environmental reconstruction. *Palaeogeography,  
581 Palaeoclimatology, Palaeoecology* 171, 97–128. doi:10.1016/S0031-0182(01)00242-5
- 582 Prasad, S., Anoop, A., Riedel, N., Sarkar, S., Menzel, P., Basavaiah, N., Krishnan, R., Fuller,  
583 D., Plessen, B., Gaye, B., Röhl, U., Wilkes, H., Sachse, D., Sawant, R., Wiesner,  
584 M.G., Stebich, M., 2014. Prolonged monsoon droughts and links to Indo-Pacific warm  
585 pool: A Holocene record from Lonar Lake, central India. *Earth and Planetary Science  
586 Letters* 391, 171–182. doi:10.1016/j.epsl.2014.01.043

- 587 Sachs, J.P., Sachse, D., Smittenberg, R.H., Zhang, Z., Battisti, D.S., Golubic, S., 2009.  
588 Southward movement of the Pacific intertropical convergence zone AD 1400–1850.  
589 Nature Geoscience 2, 519–525. doi:10.1038/ngeo554
- 590 Sano, M., Buckley, B.M., Sweda, T., 2009. Tree-ring based hydroclimate reconstruction over  
591 northern Vietnam from *Fokienia hodginsii*: eighteenth century mega-drought and  
592 tropical Pacific influence. *Climate Dynamics* 33, 331–340. doi:10.1007/s00382-008-  
593 0454-y
- 594 Singhrattna, N., Rajagopalan, B., Kumar, K.K., Clark, M., 2005. Interannual and Interdecadal  
595 Variability of Thailand Summer Monsoon Season. *Journal of Climate* 18, 1697–1708.  
596 doi:10.1175/JCLI3364.1
- 597 Sinha, A., Berkelhammer, M., Stott, L., Mudelsee, M., Cheng, H., Biswas, J., 2011a. The  
598 leading mode of Indian Summer Monsoon precipitation variability during the last  
599 millennium. *Geophysical Research Letters* 38. doi:10.1029/2011GL047713
- 600 Sinha, A., Cannariato, K.G., Stott, L.D., Cheng, H., Edwards, R.L., Yadava, M.G., Ramesh,  
601 R., Singh, I.B., 2007. A 900-year (600 to 1500 A.D.) record of the Indian summer  
602 monsoon precipitation from the core monsoon zone of India. *Geophysical Research*  
603 *Letters* 34, L16707. doi:10.1029/2007GL030431
- 604 Sinha, A., Stott, L., Berkelhammer, M., Cheng, H., Edwards, R.L., Buckley, B., Aldenderfer,  
605 M., Mudelsee, M., 2011b. A global context for megadroughts in monsoon Asia during  
606 the past millennium. *Quaternary Science Reviews* 30, 47–62.  
607 doi:10.1016/j.quascirev.2010.10.005
- 608 Tan, L., Cai, Y., Cheng, H., An, Z., Edwards, R.L., 2009. Summer monsoon precipitation  
609 variations in central China over the past 750 years derived from a high-resolution  
610 absolute-dated stalagmite. *Palaeogeography, Palaeoclimatology, Palaeoecology* 280,  
611 432–439. doi:10.1016/j.palaeo.2009.06.030
- 612 Tierney, J.E., Oppo, D.W., Rosenthal, Y., Russell, J.M., Linsley, B.K., 2010. Coordinated  
613 hydrological regimes in the Indo-Pacific region during the past two millennia.  
614 *Paleoceanography* 25, PA1102. doi:10.1029/2009PA001871
- 615 Ummenhofer, C.C., D'Arrigo, R.D., Anchukaitis, K.J., Buckley, B.M., Cook, E.R., 2013.  
616 Links between Indo-Pacific climate variability and drought in the Monsoon Asia  
617 Drought Atlas. *Climate Dynamics* 40, 1319–1334. doi:10.1007/s00382-012-1458-1
- 618 Wang, B., Clemens, S.C., Liu, P., 2003. Contrasting the Indian and East Asian monsoons:  
619 implications on geologic timescales. *Marine Geology* 201, 5–21. doi:10.1016/S0025-  
620 3227(03)00196-8
- 621 Wang, P., 2009. Global monsoon in a geological perspective. *Chinese Science Bulletin* 54,  
622 1113–1136. doi:10.1007/s11434-009-0169-4
- 623 Wang, P., Clemens, S., Beaufort, L., Braconnot, P., Ganssen, G., Jian, Z., Kershaw, P.,  
624 Sarnthein, M., 2005. Evolution and variability of the Asian monsoon system: state of  
625 the art and outstanding issues. *Quaternary Science Reviews* 24, 595–629.  
626 doi:10.1016/j.quascirev.2004.10.002
- 627 Wang, Y., Cheng, H., Edwards, R.L., He, Y., Kong, X., An, Z., Wu, J., Kelly, M.J., Dykoski,  
628 C.A., Li, X., 2005. The Holocene Asian Monsoon: Links to Solar Changes and North  
629 Atlantic Climate. *Science* 308, 854–857. doi:10.1126/science.1106296
- 630 Wannakomol, A., 2005. Soil and groundwater salinization problems in the Khorat Plateau,  
631 NE Thailand integrated study of remote sensing, geophysical and field data. Freie  
632 Universität Berlin, Berlin.
- 633 Wohlfarth, B., Klubseang, W., Inthongkaew, S., Fritz, S.C., Blaauw, M., Reimer, P.J.,  
634 Chabangborn, A., Löwemark, L., Chawchai, S., 2012. Holocene environmental  
635 changes in northeast Thailand as reconstructed from a tropical wetland. *Global and*  
636 *Planetary Change* 92–93, 148–161. doi:10.1016/j.gloplacha.2012.05.008



637 Yan, H., Sun, L., Oppo, D.W., Wang, Y., Liu, Z., Xie, Z., Liu, X., Cheng, W., 2011. South  
638 China Sea hydrological changes and Pacific Walker Circulation variations over the  
639 last millennium. *Nature Communications* 2, 293. doi:10.1038/ncomms1297  
640 Yancheva, G., Nowaczyk, N.R., Mingram, J., Dulski, P., Schettler, G., Negendank, J.F.W.,  
641 Liu, J., Sigman, D.M., Peterson, L.C., Haug, G.H., 2007. Influence of the intertropical  
642 convergence zone on the East Asian monsoon. *Nature* 445, 74–77.  
643 doi:10.1038/nature05431  
644 Zhang, P., Cheng, H., Edwards, R.L., Chen, F., Wang, Y., Yang, X., Liu, J., Tan, M., Wang,  
645 X., Liu, J., An, C., Dai, Z., Zhou, J., Zhang, D., Jia, J., Jin, L., Johnson, K.R., 2008. A  
646 Test of Climate, Sun, and Culture Relationships from an 1810-Year Chinese Cave  
647 Record. *Science* 322, 940–942. doi:10.1126/science.1163965  
648

**Table 1** Lithostratigraphic description, plant macrofossil composition of selected samples and inferred depositional environment for CP3.

Depth (m) below water surface	Lithostratigraphic description	Units	Composition of plant macro remains	Inferred depositional environment
2.00-2.02	Loose organic sediment	1	<u>Depth 2.20-2.23 m:</u> Occasional plant remains	Aquatic
2.02-2.04	Dark brown peat, compact			
2.04-2.22	Dark brown fibrous peat			
2.22-2.73	Dark brown soft fibrous peat; loose soft peat between 2.33-2.68 m	2	<u>Depth 2.54-2.57 m:</u> Large pieces of aquatic plant remains (e.g. <i>Potamogeton</i> ); Cyperaceae spp., <i>Typha</i> and Poaceae seeds.	Aquatic
			<u>Depth 2.60-2.63 m:</u> Woody fragments, plant remains, Cyperaceae spp., <i>Utricularia</i> , <i>Najas</i> and <i>Nymphoides indicum</i> seeds; macroscopic charcoal.	Aquatic– telmatic
			<u>Depth 2.63-2.66 m:</u> Plant remains; Cyperaceae spp., <i>Nymphoides indicum</i> , <i>Typha</i> and Poaceae seeds; macroscopic charcoal.	Aquatic– telmatic
			<u>Depth 2.66-2.69 m:</u> Relatively high amount of plant remains, woody remains and Cyperaceae spp. and <i>Nymphoides indicum</i> seeds.	Telmatic-terrestrial
2.73-3.04	Dark brown compact peat	3	<u>Depth 2.73-2.78 m:</u> Plant remains and Poaceae seeds.	Telmatic-terrestrial
			<u>Depth 2.98-3.04 m:</u> Coarse organic material, e.g. large wood remains; charred plant remains and Cyperaceae spp. seeds.	Terrestrial
3.04-3.34	Dark brown peaty gyttja/ coarse detritus gyttja with some fibrous peat horizons	4	<u>Depth 3.32-3.36 m:</u> Fine light roots and other plant remains; <i>Nymphaea</i> , Cyperaceae spp., <i>Typha</i> , <i>Scirpus</i> , <i>Utricularia</i> and Poaceae seeds.	Aquatic– telmatic
3.34-3.36	Transition zone between unit 5 and 4			
3.36-3.50	Dark brown fine detritus gyttja with some peaty horizons	5	<u>Depth 3.44-3.48 m:</u> Occasional plant remains	Aquatic

**Table 2**  $^{14}\text{C}$  dates for CP3. Core depth (in m) is given below the water surface. See Figure 1 for the location of the coring point. The stratigraphic units relate to those shown in Table 1. \* = undetermined

Lab ID	Core depth (m)	$^{14}\text{C}$ date BP $\pm 1 \sigma$	Dated material	Unit
UBA-23310	2.10-2.13	188 $\pm$ 24	<i>Scirpus</i> , <i>Nymphaea</i> , Cyperaceae seeds; charcoal, insects, wood piece	1
UBA-18074	2.20-2.23	299 $\pm$ 23	Seeds*, charcoal, insects	1
UBA-14635	2.54-2.57	410 $\pm$ 38	Seeds*, charcoal, wood	2
UBA-18075	2.57-2.60	434 $\pm$ 23	Seeds*, charcoal, wood	2
UBA-23756	2.60-2.63	638 $\pm$ 31	<i>Nymphaea</i> seeds, charcoal, charred plant remains, wood, bark, insects	2
UBA-19839	2.60-2.63	687 $\pm$ 23	Seeds*	2
UBA-14636	2.63-2.66	1153 $\pm$ 26	Seeds*, charcoal, wood	2
UBA-12777	2.70-2.73	1388 $\pm$ 22	Plant remains*	2
UBA-19840	2.70-2.73	1312 $\pm$ 25	Seeds*, insects, leaf fragments*	2
UBA-23311	2.73-2.78	1459 $\pm$ 28	<i>Nymphaea</i> , Cyperaceae seeds; charcoal, insects, leaf fragments*	3
UBA-23312	2.78-2.83	1777 $\pm$ 34	<i>Nymphaea</i> , Cyperaceae seeds; charcoal, wood, leaf fragment*	3
UBA-23313	2.83-2.88	1587 $\pm$ 25	<i>Nymphaea</i> , <i>Scirpus</i> , Cyperaceae seeds; charcoal, insects, leaf fragments*	3
UBA-18076	2.88-2.93	1602 $\pm$ 24	Seeds*, charcoal, insects	3
UBA-14637	2.93-2.98	1611 $\pm$ 21	Charcoal	3
UBA-19837	3.10-3.13	1625 $\pm$ 25	Seeds*, insects, leaf fragments*	4
UBA-18077	3.30-3.33	1822 $\pm$ 28	Seeds*, insects, leaf fragments*	4
UBA-14639	3.40-3.44	1873 $\pm$ 32	Small wood fragments	5
UBA-19841	3.40-3.44	2465 $\pm$ 29	Seeds*, leaf fragments, charcoal	5
UBA-16756	3.44-3.48	2083 $\pm$ 25	Seeds*, charcoal, wood, leaf fragments*	5
UBA-23283	3.48-3.52	2050 $\pm$ 28	Small wood fragments, plant remains*	5

\*Figure 1

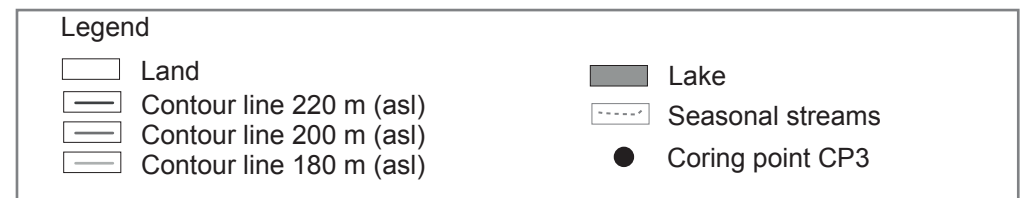
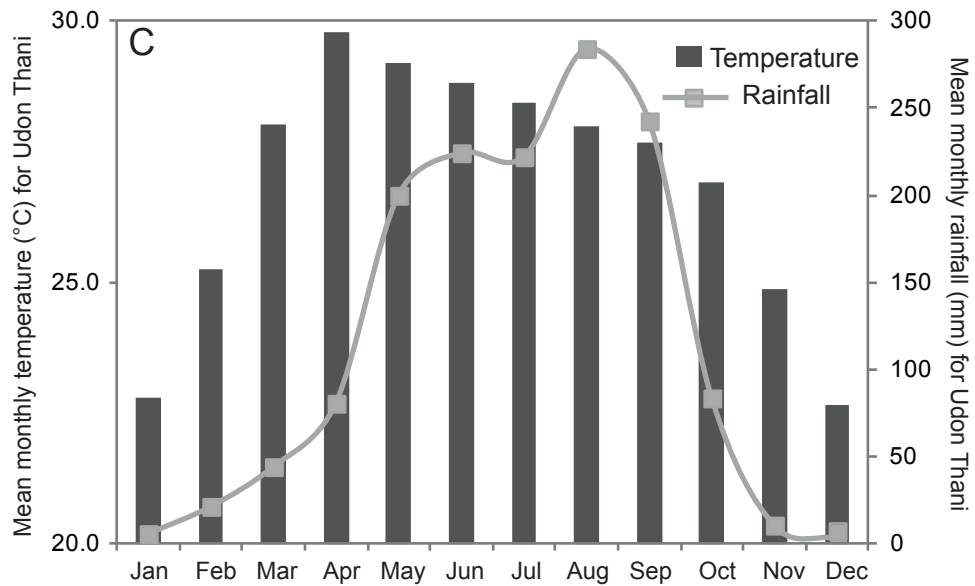
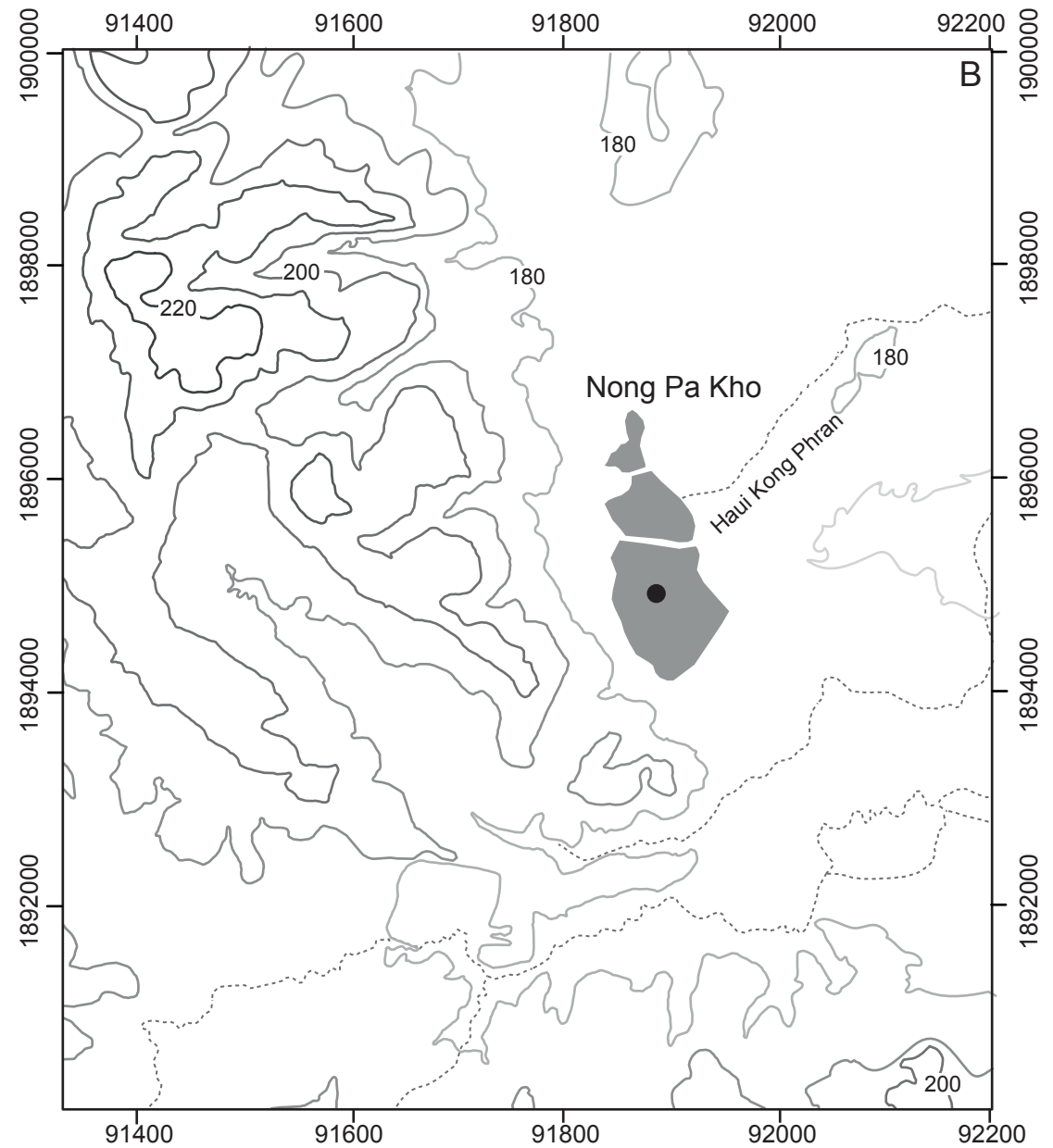


Figure 2

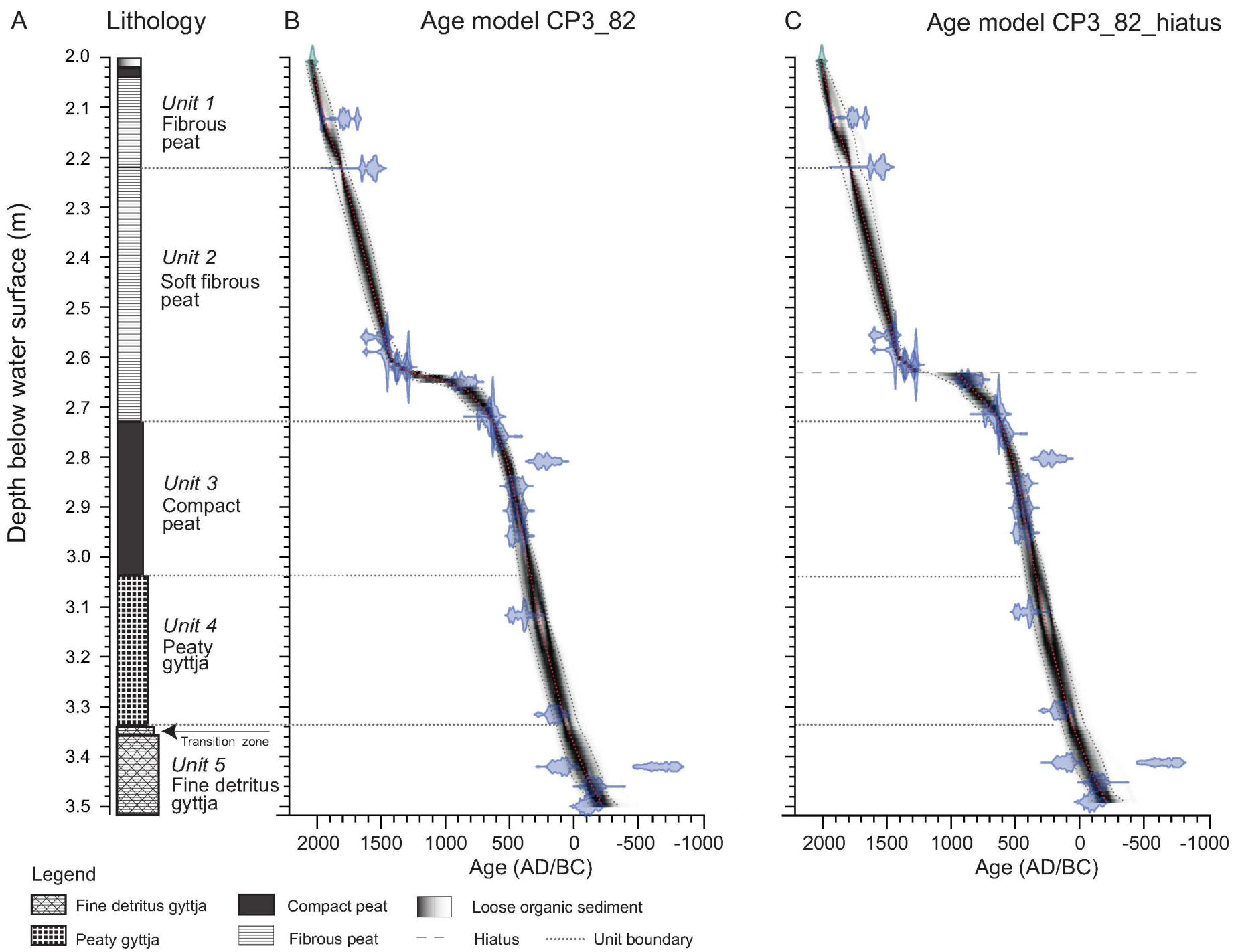
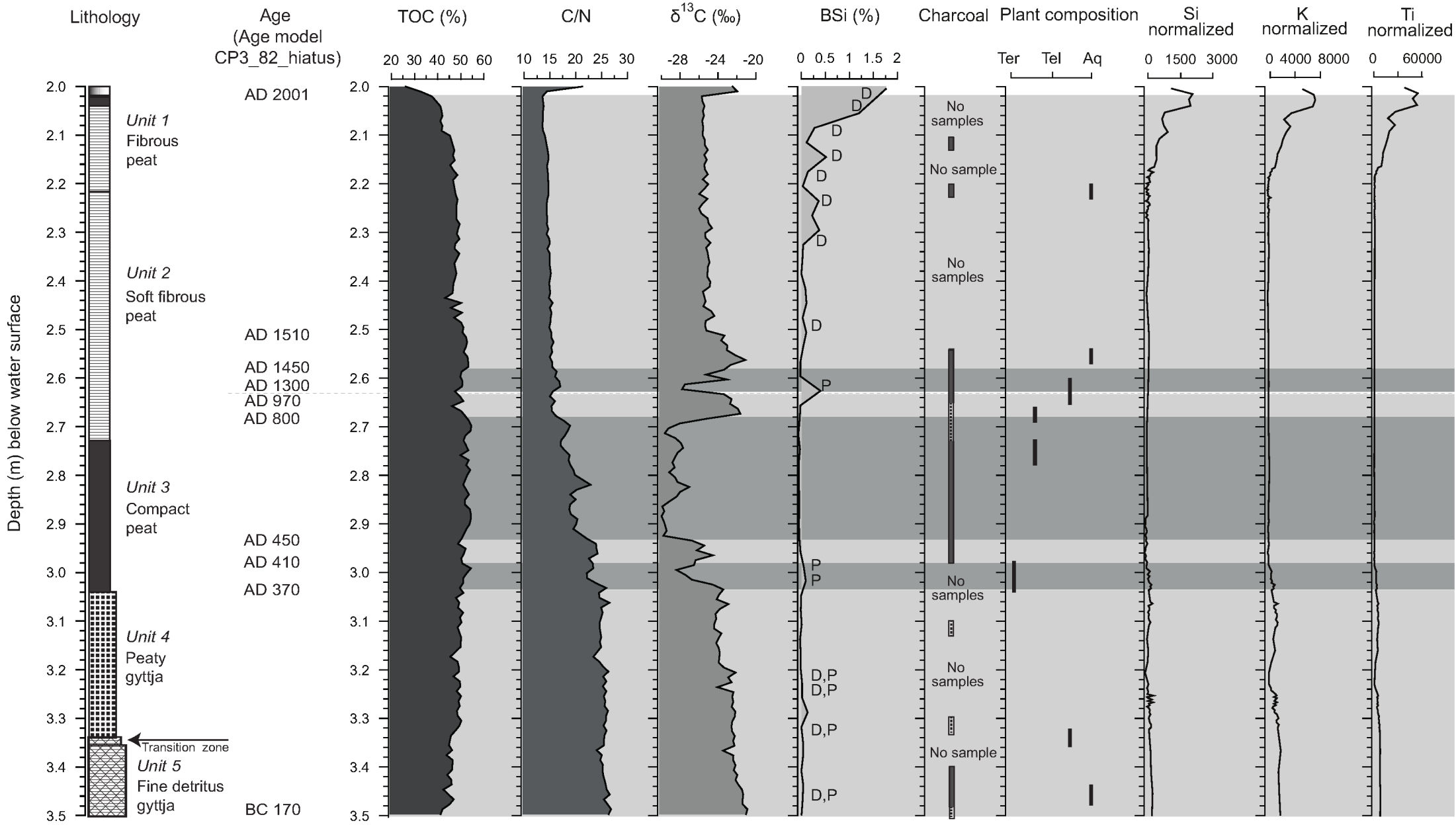


Fig. 3



**Legend**

- Fine detritus gyttja
- Peaty gyttja
- Compact peat
- Fibrous peat
- Loose organic sediment
- Hiatus
- D = Diatoms**
- P = Phytoliths**
- Ter = Terrestrial**
- Tel = Telmatic**
- Aq = Aquatic/open water**
- Charcoal present
- No charcoal present

**Figure4**  
Figure 4

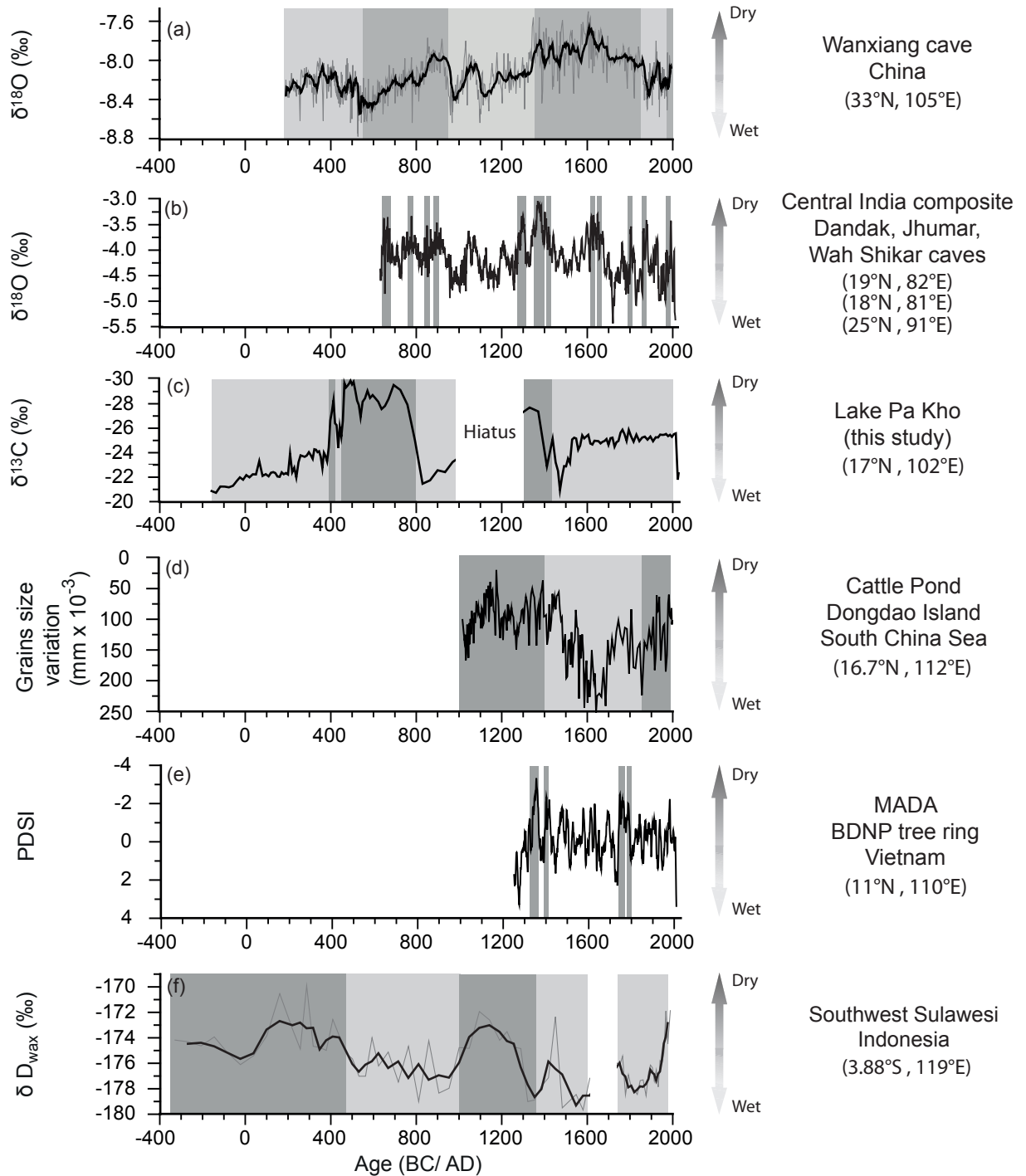
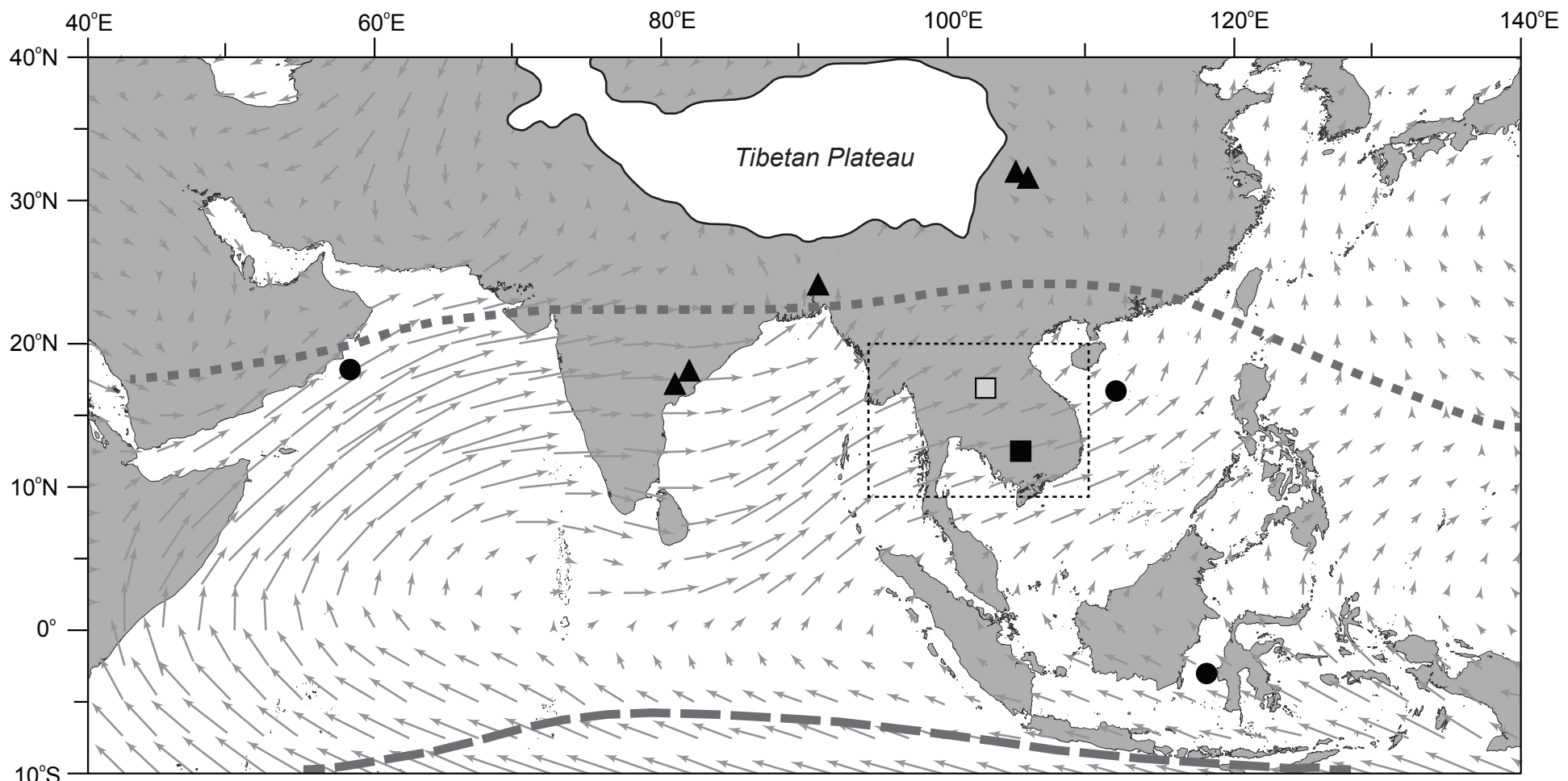


Figure 5



Legend

- Marine records
- ▲ Speleothem  $\delta^{18}\text{O}$  records
- The West Baray reservoir at Angkor, Cambodia
- Pa Kho (this study)
- ⋯ MADA tree-ring data set Indochina
- — — Mean position of the ITCZ in summer
- — — Mean position of the ITCZ in winter
- July-August wind direction